



Cellular/Molecular

Trans-synaptic Association of Vesicular Zinc Transporter 3 and Shank3 Supports Synapse-Specific Dendritic Spine Structure and Function in the Mouse Auditory Cortex

Abbey Manning,^{1,2} Philip T. R. Bender,^{1,2} Helen Boyd-Pratt,^{1,2,3} Benjamin Z. Mendelson,^{1,2}  Martin Hruska,^{1,2} and  Charles T. Anderson^{1,2}

¹Department of Neuroscience, West Virginia University School of Medicine, Morgantown, WV 26506, ²Rockefeller Neuroscience Institute, West Virginia University School of Medicine, Morgantown, WV 26506, and ³Clinical and Translational Science Institute, West Virginia University School of Medicine, Morgantown, WV 26506

Shank3 is a synaptic scaffolding protein that assists in tethering and organizing structural proteins and glutamatergic receptors in the postsynaptic density of excitatory synapses. The localization of Shank3 at excitatory synapses and the formation of stable Shank3 complexes is regulated by the binding of zinc to the C-terminal sterile-alpha-motif (SAM) domain of Shank3. Mutations in the SAM domain of Shank3 result in altered synaptic function and morphology, and disruption of zinc in synapses that express Shank3 leads to a reduction of postsynaptic proteins important for synaptic structure and function. This suggests that zinc supports the localization of postsynaptic proteins via Shank3. Many regions of the brain are highly enriched with free zinc inside glutamatergic vesicles at presynaptic terminals. At these synapses, zinc transporter 3 (ZnT3) moves zinc into vesicles where it is co-released with glutamate. Alterations in ZnT3 are implicated in multiple neurodevelopmental disorders, and ZnT3 knock-out (KO) mice—which lack synaptic zinc—show behavioral deficits associated with autism spectrum disorder and schizophrenia. Here we show that male and female ZnT3 KO mice have smaller dendritic spines and miniature excitatory postsynaptic current amplitudes than wildtype (WT) mice in the auditory cortex. Additionally, spine size deficits in ZnT3 KO mice are restricted to synapses that express Shank3. In WT mice, synapses that express both Shank3 and ZnT3 have larger spines compared to synapses that express Shank3 but not ZnT3. Together these findings suggest a mechanism whereby presynaptic ZnT3-dependent zinc supports postsynaptic structure and function via Shank3 in a synapse-specific manner.

Key words: auditory cortex; corticocollicular; dendritic spines; Shank3; Slc30a3; zinc

Significance Statement

Shank3 is a scaffolding protein that assists in the organization of glutamatergic receptors in the postsynaptic density of excitatory synapses in the brain. The structure and function of Shank3 are regulated by zinc ions. Specifically, zinc allows Shank3 to form tight sheets that assist in stabilizing the postsynaptic density. Zinc packaged by the zinc transporter 3 (ZnT3) which is released from presynaptic terminals may contribute to the function of Shank3. In this study, we found an association between ZnT3, Shank3, synaptic strength, and spine size, suggesting that zinc released from presynaptic terminals supports dendritic spine structure and function via interactions with Shank3.

Received March 26, 2024; revised May 17, 2024; accepted May 23, 2024.

Author contributions: A.M., M.H., and C.T.A. designed research; A.M., P.T.R.B., H.B.-P., B.Z.M., M.H., and C.T.A. performed research; A.M., P.T.R.B., H.B.-P., B.Z.M., and C.T.A. analyzed data; A.M. and C.T.A. wrote the paper.

We thank Hui Li and Grace Jones for their technical assistance. This work was supported by the Whitehall Foundation, 2020-05-44 (C.T.A.); the National Institute of General Medical Sciences, R35-GM138023 (C.T.A.), T32-GM132494 (A.M.), T32-GM133369 (P.T.R.B.), and P20-GM109098 (M.H.); and the Alzheimer's Association, AARG-NTF-23-1150820 (M.H.). This material is based upon work supported by the National Science

Foundation under Cooperative Agreement No. OIA-2242771 (C.T.A. and M.H.). We thank the West Virginia University (WVU) Microscope Imaging Facility, which has been supported by the WVU Cancer Institute and National Institutes of Health Grants P20-RR016440, P30-GM103488, U54-GM104942, and P20-GM103434.

The authors declare no competing financial interests.

Correspondence should be addressed to Charles T. Anderson at charles.anderson@hsc.wvu.edu or Martin Hruska at martin.hruska@hsc.wvu.edu.

<https://doi.org/10.1523/JNEUROSCI.0619-24.2024>

Copyright © 2024 the authors

Introduction

Dendritic spines are postsynaptic components of glutamatergic synapses throughout the cortex and hippocampus. Spines are plastic structures which vary in the size of the spine head, the area of the postsynaptic density, and the expression of postsynaptic proteins within the postsynaptic density (Harris and Stevens, 1989; Harris et al., 1992; Petralia et al., 1999; Takumi et al., 1999; Matsuzaki et al., 2001; Arellano, 2007; Ghani et al., 2017; Hruska et al., 2018). The structure of a spine can affect its synaptic activity (Ziv and Smith, 1996; Matsuzaki et al., 2001, 2004), and the resulting synaptic activity can affect its structure (Lissin et al., 1998; S-Q. J. Liu and Cull-Candy, 2000; Oray et al., 2006; Harvey and Svoboda, 2007).

SHANK proteins are a family of postsynaptic structural proteins that stabilize other postsynaptic structural proteins and assist in the insertion and exocytosis of membrane proteins at excitatory synapses (Du et al., 1998; M. K. Hayashi et al., 2009; Grabrucker et al., 2011b; Sala et al., 2015). SHANK3—an autism spectrum disorder-associated risk gene in human populations (Moessner et al., 2007; Boccutto et al., 2013; Uchino and Waga, 2013; Loureiro et al., 2021)—plays a role in the development of excitatory synapses (Bariselli et al., 2016; Ha et al., 2018). Shank3 can self-associate with other Shank3 proteins through the sterile alpha motif (SAM) domain (Naisbitt et al., 1999) and form tight sheets (Baron et al., 2006). These sheets are coordinated by zinc ions and cause Shank3 to become more structured (Baron et al., 2006; Gundelfinger et al., 2006). Modifying zinc levels has Shank3-dependent effects on the expression of postsynaptic proteins important for synaptic signaling (Grabrucker et al., 2011a, 2014; Arons et al., 2016; Hagemeyer et al., 2018; Vyas et al., 2020), AMPA receptor (AMPA) surface expression (Ha et al., 2018), and AMPA function (Arons et al., 2012, 2016). While the effects of exogenous zinc on the function of Shank3 are well established, whether endogenously released pools of zinc interact with Shank3 to control synaptic strength and structure is unknown.

The cortex is enriched with zinc ions which are loaded into glutamatergic vesicles by the zinc transporter 3 (ZnT3) protein (*Slc30a3*) and coreleased with glutamate during synaptic transmission (Palmiter et al., 1996; Cole et al., 1999; Salazar et al., 2005; Upmanyu et al., 2022). ZnT3 knock-out (KO) mice—which lack synaptic zinc—display cognitive and sensory deficits (Adlard et al., 2010; Martel et al., 2010, 2011; Thackray et al., 2017; Patrick Wu and Dyck, 2018; Kumar et al., 2019; Cody and Tzounopoulos, 2022) and differences in behavior and synaptic function, similar to those of Shank3 KO mice (Lavoie et al., 2011; Peça et al., 2011; Yoo et al., 2016; Upmanyu et al., 2022). Both ZnT3 and Shank3 are synaptic proteins found at excitatory, glutamatergic synapses (Palmiter et al., 1996; Du et al., 1998; Naisbitt et al., 1999; Sheng and Kim, 2000; Salazar et al., 2005; M. K. Hayashi et al., 2009; Grabrucker et al., 2011b; Sala et al., 2015; Upmanyu et al., 2022), suggesting that these proteins can coordinate to support synaptic function. Zinc ions released during transmission can move into neurons through postsynaptic zinc transporter proteins, voltage-gated calcium channels, NMDA receptors (NMDARs), and calcium-permeable AMPARs (Frederickson et al., 1989; Weiss et al., 1993; Koh and Choi, 1994; Yin and Weiss, 1995; Koh et al., 1996; Sensi et al., 1999; Jia et al., 2002; De Benedictis et al., 2021). Thus, synaptically released zinc is a prime candidate to interact with Shank3 to assist in regulation of spine morphology (Arons et al., 2012, 2016; Grabrucker et al., 2014; Hagemeyer et al., 2018; Vyas et al., 2020) and the tethering of other scaffolding proteins (Grabrucker et al., 2011a). Here we show that ZnT3 is

associated with larger dendritic spines at synapses that also contain Shank3 and that presynaptic ZnT3 expression results in stronger synaptic connections. This association between ZnT3 and Shank3 suggests that presynaptic zinc is an endogenous synapse-specific mechanism to increase the dendritic spine size and strength via Shank3.

Materials and Methods

Animal handling. Wild-type (WT) C57Bl/6 mice (Jackson Laboratory) and ZnT3 KO mice (Jackson Laboratory) were used in accordance with the animal welfare guidelines and regulations of West Virginia University, the US National Institutes of Health, and the Society for Neuroscience. All procedures were approved by the Institutional Animal Care and Use Committee of West Virginia University. WT and ZnT3 KO mice were littermates bred by heterozygous (*ZnT3*^{+/-}) pairs with a C57Bl/6 background. Both male and female mice were used in these experiments.

Stereotaxic surgeries. Mice were anesthetized with inhaled isoflurane (induction, 3% in oxygen; maintenance, 1.5% in oxygen) and secured in a stereotaxic frame (Stoelting). Core body temperature was maintained at ~37°C with a heating pad, and eyes were protected with ophthalmic ointment. Lidocaine (1%) was injected under the scalp, and an incision was made into the skin at the midline to expose the skull. Using a 27 gauge needle as a scalpel, a small craniotomy (~0.4 mm diameter) was made over the inferior colliculus at coordinates 1.3 mm posterior and 1.0 mm lateral to the lambda. Borosilicate glass pipettes (VWR International) were pulled to a shallow taper (length, >1 cm; tip diameter, ~30 μm) and advanced into the region of interest at an angle ~25° off the horizontal plane. Injection pipettes were backfilled with mineral oil (Sigma-Aldrich) and filled with AAV-hSyn1-GCaMP6s-2A-nls-dTomato, pGP-AAV-syn-jGCaMP8m-WPRE (titer 5e¹² – 5e¹³ genome copies/ml, Addgene), or cholera toxin subunit B (CTB) conjugated to Alexa Fluor 555 (CTB-555, 1 mg/μl, Thermo Fisher Scientific). They were connected to 5 μl glass syringes (Hamilton) via capillary tubing and controlled with syringe pumps (World Precision Instruments). Pipettes were inserted 0.55 mm deep into the craniotomy, and 0.4 μl of CTB-555 was injected at 0.2 μl per minute for 2 min, or 0.9 μl of adeno-associated virus (AAV) was injected at 0.3 μl per minute for 3 min. After injections, the pipettes were left in place for 2 min prior to removal, and then the scalp of the mouse was closed with cyanoacrylate adhesive. Mice received an injection of nonsteroidal anti-inflammatory drug meloxicam during the injection procedure and a diet of meloxicam tablets (Bio-Serv) for 72 h after surgery. Mice were monitored for signs of postoperative stress and pain.

Western blot. WT and ZnT3 KO mice were deeply anesthetized, euthanized, and had their brains removed. The brains were dissected, and both hemispheres of the cortex were removed, homogenized, and sonicated. Samples were incubated with a RIPA buffer (Sigma-Aldrich) and a protease inhibitor cocktail (1 mM AEBSF, 800 nM aprotinin, 50 μM bestatin, 15 μM E-64, 20 μM leupeptin, 10 μM pepstatin A, 5 mM EDTA; Thermo Fisher Scientific) on ice for 30 min and centrifuged for 10 min at 12 k RPM and 4°C, and the supernatant was saved. Using the Pierce BCA Protein Assay Kit (Thermo Fisher Scientific), the concentration of each sample was determined, and sample concentrations were then reduced to the lowest sample concentration using Milli-Q ultrapure water. Samples were then mixed 1:1 with 5% β-mercaptoethanol (Thermo Fisher Scientific) in a 2× Laemmli sample buffer (Bio-Rad Laboratories) and boiled for 5 min at 100°C. Samples were separated on 4–20% Mini-PROTEAN TGX Gels (Bio-Rad Laboratories) and transferred to 0.2 μm PVDF membrane (Bio-Rad Laboratories) using a 25 mM Tris, 192 mM glycine, and 0.1% (w/v) SDS buffer (Bio-Rad Laboratories). The membrane was first blocked using 3% bovine serum albumin (BSA, G-Biosciences) for 1 h at room temperature and then incubated with rabbit anti-ZnT3 primary antibody in 3% BSA (1:1,000, Synaptic Systems, 197 003) overnight at 4°C. The membrane was washed three times in a phosphate-buffered saline

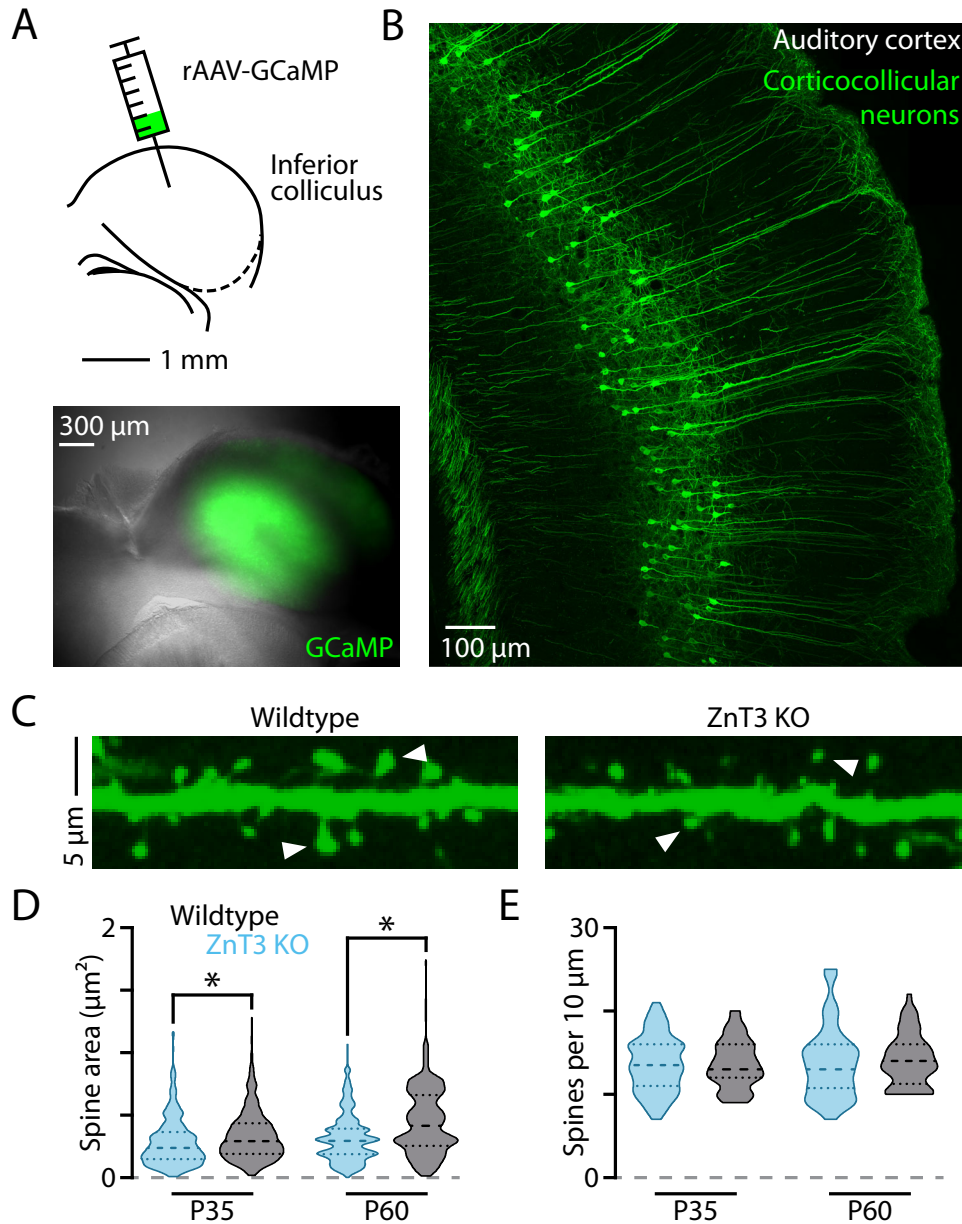


Figure 1. ZnT3 KO mice have smaller spines than WT mice. **A**, Top, A diagram showing the experimental injection scheme for labeling corticocollicular neurons in the auditory cortex. Bottom, An example image of the right inferior colliculus with a retrograde AAV encoding GCaMP (rAAV-GCaMP) injection. **B**, An example image of corticocollicular neurons labeled with rAAV-GCaMP in the right auditory cortex of a WT mouse. **C**, Example images of Layer 2/3 apical dendritic spines labeled with rAAV-GCaMP (white arrows) in a WT (left) and ZnT3 KO (right) mouse. **D**, The spine area for WT (black) and ZnT3 KO (cyan) mice at P35 (left) and P60 (right; P35, $p = 3.086 \times 10^{-6}$; WT, $n = 590$ spines; ZnT3 KO, $n = 361$ spines; P60, $p = 4.894 \times 10^{-20}$; WT, $n = 740$ spines; ZnT3 KO, $n = 569$ spines; Mann–Whitney U test). **E**, Spine density per 10 μm of dendrite for WT (black) and ZnT3 KO (cyan) mice at P35 (left) and P60 (right; P35, $p = 0.927$; WT, $n = 60$ ROI; ZnT3 KO, $n = 60$ ROI; P60, $p = 0.724$; WT, $n = 70$ ROI; ZnT3 KO, $n = 50$ ROI; unpaired t test).

(PBS, Fisher BioReagents) with 0.1% Tween 20 (Sigma-Aldrich) for 15 min. The membrane was then incubated with goat anti-rabbit secondary antibody conjugated to horse radish peroxidase (1:2,000, Bio-Rad Laboratories, 1721019) in PBS with Tween 20 (PBST) for 1 h at room temperature and washed three times for 15 min with PBST. SuperSignal West Pico PLUS Stable Peroxide (Thermo Fisher Scientific) was mixed 1:1 with SuperSignal West Pico PLUS Luminol/Enhancer (Thermo Fisher Scientific) and placed gently over the membrane and imaged using an Amersham Imager 680 (GE Life Sciences). After imaging, the membrane was rinsed with PBST, incubated with rabbit anti-glyceraldehyde 3-phosphate dehydrogenase (GAPDH; 1:1,000, Bio-Rad Laboratories, VPA00187) in 3% BSA overnight at 4°C, and then washed three times with PBST for 15 min. The membrane was incubated with goat anti-rabbit secondary antibody conjugated to horse

radish peroxidase (1:2,000, Bio-Rad Laboratories, 1721019) in PBST for 1 h at room temperature, washed three times for 15 min with PBST, and then imaged as previously described. To quantify the bands, the Western blots were analyzed using Fiji (Schindelin et al., 2012). The intensity of each band was measured through Fiji's automatic measuring tool. The background surrounding each band was measured the same way and subtracted from the band intensity. The resulting band intensities were then made into a ratio of ZnT3 band intensity/GAPDH band intensity.

Perfusions. Male and female Postnatal Day (P) 35 and P60 WT and ZnT3 KO mice were anesthetized and perfused transcardially using carbonated artificial cerebral spinal fluid (ACSF) containing the following (in mM), 130 NaCl, 3 KCl, 2.4 CaCl₂, 1.3 MgCl₂, 20 NaHCO₃, 3 HEPES,

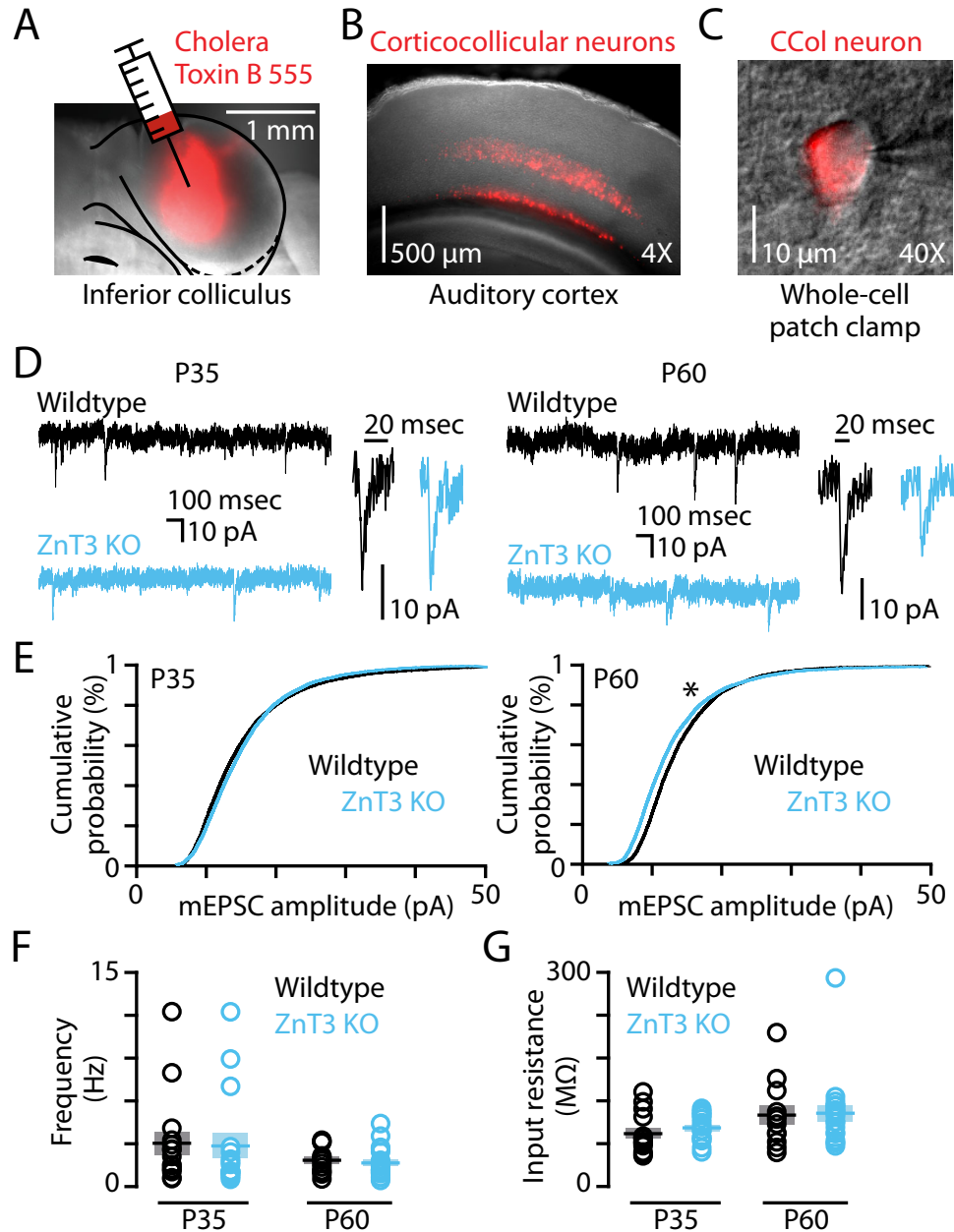


Figure 2. ZnT3 KO mice have smaller miniature EPSC amplitudes than WT mice at P60 but not P35. **A**, An image of the inferior colliculus of a mouse injected with the retrograde tracer CTB conjugated to Alexa Fluor 555 (red) with an overlaid diagram showing the injection scheme. **B**, An image of the auditory cortex of a mouse with corticocollicular neurons retrogradely labeled with CTB-555 (red). **C**, An image of a CTB-555-labeled corticocollicular (CCol) neuron in Layer 5 in whole-cell patch-clamp configuration. **D**, Example mEPSC recordings from P35 (left) and P60 (right) WT (top, black) and ZnT3 KO (bottom, cyan) mice, with representative mEPSCs from both groups (to the right of traces). **E**, Cumulative distribution of mEPSC amplitudes recorded from P35 (left) and P60 (right) WT (black) and ZnT3 KO (cyan) mice (P35: $p = 0.4896$; WT, $n = 4,500$ events from 15 cells from 11 mice; ZnT3 KO, $n = 4,800$ events from 16 cells from 11 mice; P60: $p = 1.115 \times 10^{-7}$; WT, $n = 3,600$ events from 12 cells from 11 mice; ZnT3 KO, $n = 6,000$ events from 20 cells from 8 mice. One-way ANOVA with Holm–Sidak’s multiple-comparison test). **F**, Frequency of mEPSCs recorded from WT (black) mice and ZnT3 KO (cyan) mice at P35 (left) and P60 (right). Darker lines represent the mean value; lighter shaded area represents SEM (P35: $p = 0.8817$; WT, $n = 15$ cells from 11 mice; ZnT3 KO, $n = 16$ cells from 11 mice; P60: $p = 0.6048$; WT, $n = 12$ cells from 11 mice; ZnT3 KO, $n = 20$ cells from 8 mice; unpaired *t* test). **G**, Input resistance of corticocollicular neurons during mEPSC recordings from WT (black) mice and ZnT3 KO (cyan) mice at P35 (left) and P60 (right). Darker lines represent the mean value; lighter shaded area represents SEM (P35: $p = 0.3448$; WT, $n = 15$ cells from 11 mice; KO, $n = 16$ cells from 11 mice; P60: $p = 0.8836$; WT, $n = 12$ cells from 11 mice; KO, $n = 20$ cells from 8 mice; unpaired *t* test).

and 10 D-glucose [saturated with 95% O₂/5% CO₂ (vol/vol), ~300 mOsm], pH 7.25–7.35, followed by 4% paraformaldehyde (PFA) with 0.0028% glutaraldehyde in PBS. Brains were immediately removed and placed into PFA overnight. Brains were then cryopreserved in 30% sucrose in PBS and sectioned coronally at 25 μm on a microtome (Thermo Fisher Scientific Sliding Microtome Microm HM450) with a BFS-40MPA Freezing Stage (Physitemp). Sections were stored free-floating in 0.01% sodium azide in PBS at 4°C.

Immunohistochemistry. Sections from the auditory cortex were first blocked for 1 h at room temperature in a blocking buffer (1% BSA, 10% fetal bovine serum, 1% Triton X-100 in PBS). Sections were then incubated for 48 h at 4°C with primary antibody [chicken anti-GFP, 1:1,000, Abcam, 13970; guinea pig anti-bassoon, 1:200, Synaptic Systems, 141 004; mouse IgG1 anti-Shank1, 1:500, Abcam, 94576; mouse IgG2b anti-Shank3, 1:500, Abcam, 93607; alpaca anti-postsynaptic density 95 (PSD-95) ATTO647N, 1:500, NanoTag Biotechnologies,

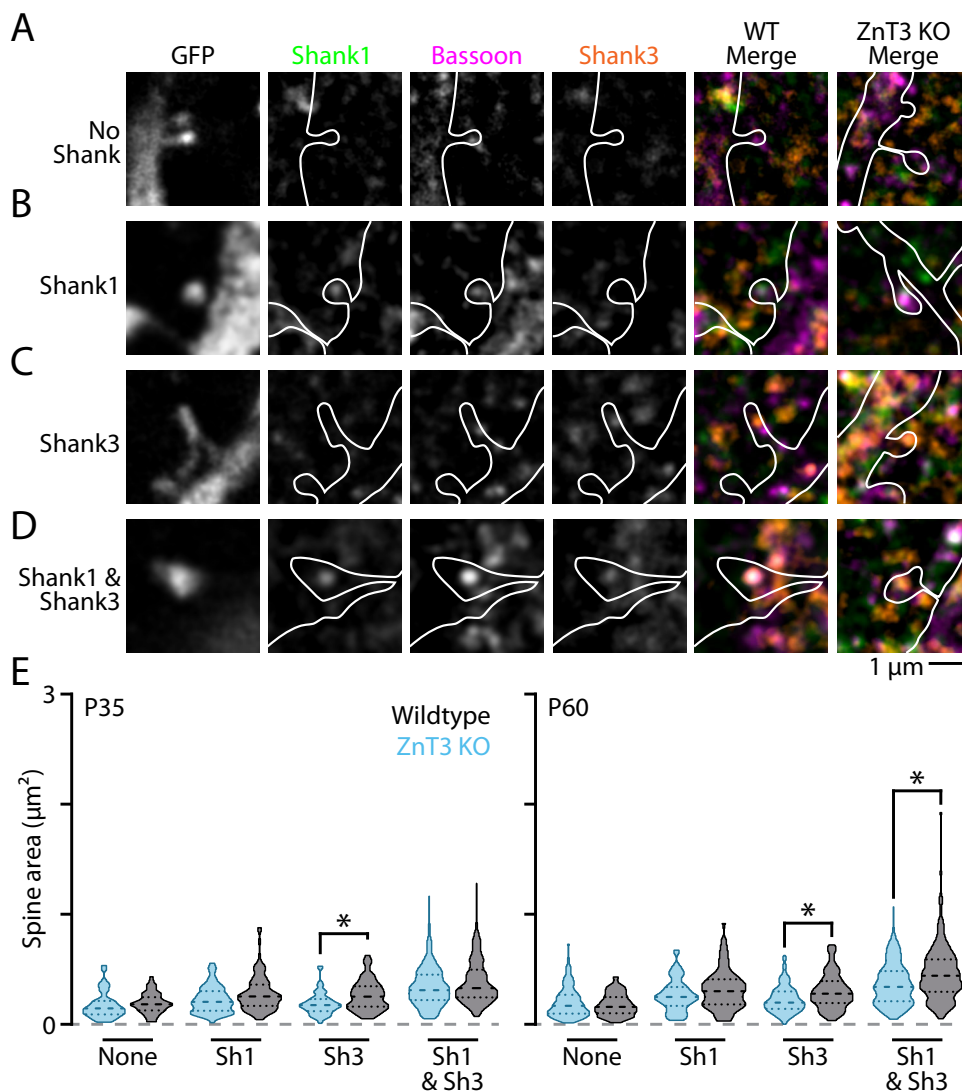


Figure 3. Spines with Shank3 are larger in WT mice. **A**, An example image of a synapse in Layer 2/3 that does not express any Shank proteins. White outline indicates the dendrite and dendritic spine. Merged image shows Shank1 (green), bassoon (magenta), and Shank3 (orange) stains. **B**, An example image of a synapse that only expresses Shank1. The same color scheme as in **A**. **C**, An example image of a synapse that only expresses Shank3. The same color scheme as in **A**. **D**, An example image of a synapse that expresses both Shank1 and Shank3. The same color scheme as in **A**. **E**, The spine area for WT (black) and ZnT3 KO mice (blue) at P35 (left) and P60 (right) for each condition (P35 none: $p > 0.999$; WT, $n = 67$ spines; ZnT3 KO, $n = 72$ spines; P35 Shank1: $p = 0.210$; WT, $n = 97$ spines; ZnT3 KO, $n = 94$ spines; P35 Shank3: $p = 0.0305$; WT, $n = 58$ spines; ZnT3 KO, $n = 60$ spines; P35 Shank1/Shank3: $p = 0.652$; WT, $n = 195$ spines; ZnT3 KO, $n = 203$ spines; P60 none: $p > 0.999$; WT, $n = 113$ spines; ZnT3 KO, $n = 133$ spines; P60 Shank1: $p = 0.546$; WT, $n = 77$ spines; ZnT3 KO, $n = 105$ spines; P60 Shank3: $p = 0.00780$; WT, $n = 97$ spines; ZnT3 KO, $n = 107$ spines; P60 Shank1/Shank3: $p = 0.00220$; WT, $n = 160$ spines; ZnT3 KO, $n = 221$ spines; Kruskal–Wallis test with Dunn’s multiple comparisons).

N3702-At647N-L; rabbit anti-ZnT3, 1:1,000, Synaptic Systems, 197 003] in a blocking buffer and washed three times for 10 min in PBS. Primary antibodies for GFP (Wang et al., 2023; Xue et al., 2023), bassoon (C. Liu et al., 2018; De Rossi et al., 2020; Actor-Engel et al., 2021; Feng et al., 2021; Kang et al., 2021; Hruska et al., 2022), Shank1 (Collins and Galvez, 2018), Shank3 (Man et al., 2020), and PSD-95 (Kilisch et al., 2023) have all been previously validated through cell lines, KO models, or use of shRNA. Sections were incubated with secondary antibody (goat anti-chicken Alexa Fluor 488, Jackson ImmunoResearch Laboratories, 103-545-1555; goat anti-guinea pig Alexa Fluor 555, Invitrogen, A-21435; goat anti-mouse IgG1 Alexa Fluor 594, Jackson ImmunoResearch Laboratories, 115-587-158; goat anti-mouse IgG1 Alexa Fluor 555, Invitrogen, A-21127; goat anti-mouse IgG2b Alexa Fluor 647N, Rockland Immunochemicals, 610-156-042; goat anti-rabbit Alexa Fluor 594, Jackson ImmunoResearch Laboratories, 111-585-144) in a blocking buffer (1:500) for 2 h at room temperature, washed three times in PBS for 10 min, washed two times in 0.1 M phosphate buffer

for 5 min, and mounted to glass slides with ProLong Glass Antifade Mountant (Invitrogen) and covered with a No. 1.5 glass coverslip.

Fluorescent imaging and analysis. The $25 \times 25 \mu\text{m}$ confocal Z-stacks of dendrites were obtained using a Zeiss LSM 710 confocal with a $63\times$ oil immersion objective or a Leica STELLARIS 8 with $40\times$ and $100\times$ oil immersion objectives. Z-stacks were analyzed using Fiji (Schindelin et al., 2012). A Gaussian blur (sigma of $0.04 \mu\text{m}$) was applied to each image to filter out noise. To determine the spine size, the head of each spine within each image was selected and thresholded. The area of each spine head was determined automatically using Fiji’s measurement tool. The presence of a protein at each synapse was determined through a statistical measure of puncta fluorescence against the background fluorescence of a $1 \mu\text{m} \times 1 \mu\text{m}$ area around the puncta. Expression was defined as the mean puncta fluorescence intensity being greater than the mean $+ 2 \times$ standard deviation of the mean background fluorescence intensity. Fluorescence intensity was determined automatically using Fiji’s measurement tool. The

300 μm \times 250 μm Z-stacks of the mouse right auditory cortex were obtained using a Nikon E800 microscope with a 4 \times dry objective. The 10 μm sections of dendrites within Layer 2/3 were selected, and spine density was counted manually through Fiji. All analysis was performed blinded on sex, genotype, and age. Sections stained with just ZnT3 were imaged using an Olympus MVX MacroView microscope with a Hamamatsu ORCA_Flash4.0 v2 sCMOS camera.

Brain slice electrophysiology. Acute brain slice experiments were performed 4–7 d postinjection with CTB-555. Slices were examined during experiments to confirm accurate placement of the injection sites. Brain slices of the auditory cortex were cut in chilled carbogenated choline-based solution of the following composition (in mM): 110 choline chloride, 25 NaHCO₃, 25 D-glucose, 11.6 sodium ascorbate, 3.1 sodium pyruvate, 2.5 KCl, 0.5 CaCl₂, and 7 MgCl₂. Brain slice electrophysiology experiments were carried out using carbogenated ACSF with the following composition (in mM), 130 NaCl, 3 KCl, 2.4 CaCl₂, 1.3 MgCl₂, 20 NaHCO₃, 3 HEPES, and 10 D-glucose, saturated with 95% O₂/5% CO₂ (vol/vol), pH 7.25–7.35, ~300 mOsm. All solutions were continuously bubbled with carbogen. Contaminating zinc was removed from the ACSF for all experiments by stirring the ACSF with Chelex 100 Resin (Bio-Rad Laboratories) for 1 h. High-purity CaCl₂ and MgCl₂ salts (99.995% purity; Sigma-Aldrich) were added to the ACSF after the Chelex 100 resin was filtered using Nalgene Rapid-Flow filters lined with polyethersulfone (0.2 μm pore size). All plastic and glassware were washed with 5% high-purity nitric acid. Mice were first anesthetized with isoflurane and then immediately decapitated. Brains were rapidly removed, and coronal slices (300 μm) of the cortex were prepared in chilled choline chloride cutting solution using a vibratome (VT1200 S; Leica). Slices were then transferred into a holding chamber of carbogenated ACSF and incubated for ~30 min at 35°C and then incubated at room temperature for ~30 min before electrophysiological experiments were performed. For electrophysiological experiments, slices were transferred into the recording chamber and perfused with carbogenated ACSF at a rate of 1–2 ml/min. Recordings were performed at 30–32°C using an in-line heating system (Warner Instruments). Corticocollicular neurons were identified by their labeling with the retrograde labeler CTB conjugated to Alexa Fluor 555 (Thermo Fisher Scientific). Electrophysiological recordings were made using an amplifier (MultiClamp 700B, Axon Instruments), a digital-to-analog converter (USB-6229, National Instruments), and ephus (Suter et al., 2010). Voltage-clamp recordings were conducted using borosilicate pipettes (Warner Instruments) pulled to tip resistances of 3–5 M Ω (Sutter Instrument) filled with a cesium-based internal solution with the following composition (in mM), 128 cesium-methanesulfonate, 10 HEPES, 4 MgCl₂, 4 Na₂ ATP, 0.3 Tris-GTP, 10 Tris-phosphocreatine, 0.5 cesium-EGTA, 3 Na-ascorbate, and 1 QX314 (303 mOsm), pH 7.23, at –70 mV holding potential. Tetrodotoxin (TTX; 500 nM) was bath applied.

Experimental design and statistical analysis. The number of replicates per experiment and their definitions are listed in the figure legends. Electrophysiological data were sampled at 10 kHz and low-pass filtered at 2–4 kHz. Series resistance was monitored during the experiment by giving brief –5 mV voltage steps at regular intervals during the recording session. Input resistance was continuously monitored during recordings. Miniature excitatory postsynaptic currents (mEPSCs) were recorded at –70 mV. Events were detected and analyzed using Mini Analysis (Synaptosoft). Only neurons with root mean square (RMS) of membrane current noise <2.5 and series resistance >10 M Ω and <25 M Ω with <15% change during the recording time were included in the analysis. The threshold for mEPSC detection was set to three times the RMS noise. The first 300 nonoverlapping events with rise times less than or equal to 3 ms were used to estimate the mEPSC amplitude distribution and frequency. Neurons with a negative correlation between the mEPSC amplitude and rise time were excluded. Events were recorded over 5–10 min after stability was achieved during recordings in TTX. Experiments using ZnT3 KO mice were performed blind to the age, sex, and genotype of the animal. Experiments using only WT mice

were performed blind to age and sex. Analysis was performed with Fiji (Schindelin et al., 2012), MATLAB (MathWorks), and Prism (GraphPad Software). Based on statistical approaches reported in recent studies of spine morphology (Cane et al., 2014; Hruska et al., 2018, 2022; Ishii et al., 2018; Borczyk et al., 2019), analysis of the spine size was performed using the total number of spines as the *n* for tests of statistical significance. The number of spines and animals used for each comparison are listed in the [Extended Data](#). For statistical comparisons, a student unpaired *t* test was used if the group data passed Lilliefors test for normality (Figs. 1E, 2F,G, 4A). If the group data were not normally distributed, a Kruskal–Wallis *H* test was used to compare three or more groups (Figs. 3E, 4F, 5C), and a Mann–Whitney *U* test (Fig. 1D) was used to compare two groups. A statistical comparison was determined to be significant if the *p* value was <0.05 for single comparisons or by use of Dunn's multiple-comparison test for multiple comparisons. Statistically significant differences are denoted in figures with an asterisk (*), and *p* values are listed in the figure legends. Statistical analyses were performed using Prism (GraphPad Software) and Excel (Microsoft). Bar plots show the mean with error bars representing \pm standard error of the mean (SEM). Violin plots show the distribution of the data with a dashed line representing the median and dotted lines representing the upper and lower quartiles.

Results

Dendritic spines are smaller in ZnT3 KO mice

Because smaller dendritic spines are associated with changes in behavior and synaptic function that are also observed in ZnT3 KO mice (Lavoie et al., 2011; Yoo et al., 2016), we hypothesized that these mice would have altered dendritic spine morphology. To address this question, we performed stereotaxic injections of a retrograde AAV-GCaMP (see Materials and Methods) in the right inferior colliculus of age-matched, sex-matched littermates of WT and ZnT3 KO mice to induce the expression of GCaMP in Layer 5 corticocollicular neurons in the auditory cortex (Fig. 1A,B). We focused on these neurons because they receive a variety of corticocortical inputs at synapses that corelease zinc and glutamate and that express presynaptic ZnT3 (Cole et al., 1999; Brown and Dyck, 2004; Petreanu et al., 2007; Hooks et al., 2011; Upmanyu et al., 2022; Bender et al., 2023). In particular, these neurons receive strong input from Layer 2/3 intratelencephalic-type neurons (Joshi et al., 2015; Bender et al., 2023) which contain high levels of vesicular zinc (Palmiter et al., 1996; Cole et al., 1999; Brown and Dyck, 2004; McAllister and Dyck, 2017a,b). Fourteen days postinjection, the mice were perfused, and their brains were fixed and sectioned. Immunohistochemical staining for GFP was performed to boost the fluorescence intensity of GCaMP (see Materials and Methods). Although GCaMP can be used to measure changes in neuronal calcium levels (T-W. Chen et al., 2013; Bender et al., 2023), here, we used it as a structural marker for dendritic spines due to its bright GFP-based fluorescence signal (Harvey and Svoboda, 2007; Durand et al., 2012; T-W. Chen et al., 2013; He et al., 2018). After staining, sections were mounted, and fluorescent images were obtained (see Materials and Methods). Because of the high density of spines but low density of dendrites, spines were selected in Layer 2/3 of the auditory cortex (Chang and Kawai, 2018) and analyzed using a fluorescence threshold measure of the spine head area (Hruska et al., 2018, 2022; Fig. 1C). All image acquisition, segmentation, and analysis were performed blind to the age, genotype, and sex of the animals (see Materials and Methods). We found that dendritic spines in ZnT3 KO mice were significantly smaller than in WT mice at P35 (Fig. 1D). Because the dendritic spine size increases with age (Dumitriu et al., 2010; Orner et al., 2014; Young et al., 2014), this result could reflect a developmental delay that might normalize with more

time, or it could be a persistent deficit in these animals. To distinguish between these possibilities, we performed similar experiments in mice at P60. In older animals, there was a more pronounced deficit in spine sizes in ZnT3 KO mice compared with those in WT mice, suggesting that the deficits in spine sizes are progressively more severe with age. There was not a change in spine density between WT and ZnT3 KO mice at either age (Fig. 1E).

Synaptic strength is reduced in ZnT3 KO mice

Because larger dendritic spines are associated with stronger synaptic connections (Engert and Bonhoeffer, 1999; Maletic-Savatic et al., 1999; Grutzendler et al., 2002; Matsuzaki et al., 2004; Harvey and Svoboda, 2007; Y. Yang et al., 2008; Peça et al., 2011; Durand et al., 2012), we hypothesized that the smaller dendritic spines we observed in ZnT3 KO mice would be associated with weaker synaptic inputs in these animals. To test this hypothesis, we performed whole-cell patch-clamp recordings from corticocollicular neurons in acute brain slices from WT and ZnT3 KO mice. We retrogradely labeled Layer 5 corticocollicular neurons by performing a stereotaxic injection of retrograde tracer CTB conjugated to Alexa Fluor 555 (CTB-555) into the right inferior colliculus of both WT and ZnT3 KO mice (Fig. 2A,B). Postinjection, acute brain slices containing the auditory cortex were prepared at P35–P37 and P60–P63 for both genotypes and sexes. Whole-cell patch-clamp recordings were performed under voltage-clamp conditions in the presence of TTX to block sodium channels and isolate nonaction potential-mediated mEPSCs (Fig. 2C,D). At P35, there was no significant difference in mEPSC amplitude between WT and ZnT3 KO mice, but at P60, ZnT3 KO mice had smaller mEPSC amplitudes than WT mice (Fig. 2E). No difference in mEPSC frequency was observed between all groups (Fig. 2F), and there were no significant differences in the input resistances between WT and ZnT3 KO mice (Fig. 2G). These results are consistent with the reduced spine size and normal spine density in the neurons and suggest that ZnT3 enhances synaptic strength in part by increasing the spine size. Together, these data show that the loss of the presynaptic protein ZnT3 is associated with altered spine structure and spine function.

Shank3 is associated with smaller dendritic spines in ZnT3 KO mice

While multiple studies have investigated how free zinc regulates the postsynaptic spine through interactions with zinc-sensitive structural proteins (Grabrucker et al., 2011a, 2014; Arons et al., 2012, 2016; Hagemeyer et al., 2018; Vyas et al., 2020), none have directly linked synaptic zinc provided by ZnT3 to these mechanisms. We hypothesized that a likely link between presynaptic zinc release and postsynaptic morphology could be zinc-sensitive structural proteins. Because ZnT3 KO mice have a loss of zinc ions in synaptic vesicles and synaptic clefts and a ~20% reduction in total zinc in the cortex (Cole et al., 1999), we hypothesized that the lack of ZnT3-dependent synaptic zinc in ZnT3 KO mice could have preferential effects on the structure of Shank3-containing dendritic spines. To address this hypothesis, we performed immunohistochemical staining for Shank3; Shank1, a zinc-insensitive Shank protein; and bassoon, a presynaptic protein that assists in tethering vesicles at the active zone (Takao-Rikitsu et al., 2004; Tom Dieck et al., 2005; Magupalli et al., 2008; Fig. 3A–D). Following labeling of these synaptic proteins, we imaged dendritic spines as above, and protein expression was determined by non-biased fluorescence intensity thresholding (see Materials and

Methods). At P35, synapses containing only Shank3 with no Shank1 correlated with smaller spines in ZnT3 KO mice compared with those in WT mice (Fig. 3E). Consistent with the more pronounced reduction in the spine size at P60, the Shank3-associated deficiency was more pronounced at this age, and the presence of Shank1 was not sufficient to prevent the reduction in the spine size at synapses containing Shank3 (Fig. 3E). Together, these findings suggest that the average overall reduction in the spine size in ZnT3 KO mice (Fig. 1D) is mediated by spines at synapses that express Shank3.

Postsynaptic Shank3 and presynaptic ZnT3 associate with larger dendritic spines in WT mice

Thus far, we have compared synapses between WT and ZnT3 KO littermates. Next, we hypothesized that the principles relating ZnT3 to the spine size would also exist in WT mice, which have a mix of ZnT3-containing (ZnT3⁺) and ZnT3-lacking (ZnT3⁻) synapses. To address this hypothesis, we performed immunohistochemical staining for bassoon, PSD-95 (a postsynaptic scaffolding protein that binds directly to membrane proteins; Kornau et al., 1995; Kim and Sheng, 2004; Bats et al., 2007; X. Chen et al., 2015; Won et al., 2016, 2017), and ZnT3. We verified that this ZnT3 antibody is highly selective for ZnT3 because there is robust signal in the WT brain tissue and a lack of signal in the ZnT3 KO brain tissue, as assessed with Western blot and immunohistochemical analysis (Fig. 4A,B). Dendritic spines in Layer 2/3 of the auditory cortex were imaged, and protein expression at synapses and spine size were analyzed as above (Fig. 4C,D). We found that ~80% of synapses contained ZnT3 at both P35 and P60 (Fig. 4E), confirming that WT animals have a mix of ZnT3⁺ and ZnT3⁻ synapses. Consistent with the relationship between ZnT3 and larger spines observed above, spines at synapses that contained ZnT3 (ZnT3⁺) were significantly larger than spines at synapses that did not contain ZnT3 (ZnT3⁻) in WT mice (Fig. 4F). These results suggest that the expression of ZnT3 at a synapse is associated with larger spine sizes. Next, we hypothesized that ZnT3⁺ synapses with Shank3 would also associate with larger dendritic spines in WT mice. To address this hypothesis, WT mouse brain sections were labeled for Shank1, Shank3, and ZnT3 (Fig. 5A,B). At P35, Shank proteins did not correlate with larger spines at ZnT3⁺ synapses; however, at P60, Shank3-containing, ZnT3⁺ synapses were associated with significantly larger dendritic spines (Fig. 5C). Together, these data suggest that ZnT3-dependent zinc can interact with zinc-sensitive Shank3, leading to larger dendritic spines at specific cortical synapses (Fig. 5C).

Discussion

The structure and function of dendritic spines is tightly linked, where the structure of a spine can affect its synaptic activity and vice versa (Ziv and Smith, 1996; Lissin et al., 1998; S-Q. J. Liu and Cull-Candy, 2000; Matsuzaki et al., 2001, 2004; Oray et al., 2006; Harvey and Svoboda, 2007). Here, we show that ZnT3 KO mice have both smaller spines and mEPSCs compared with WT mice, suggesting that presynaptic zinc affects postsynaptic structure in addition to its established roles in shaping synaptic signaling through modulation of glutamate receptor function (Pan et al., 2011; Vergnano et al., 2014; Anderson et al., 2015; Kalappa et al., 2015; Kalappa and Tzounopoulos, 2017; Morabito et al., 2022; Bender et al., 2023). Additionally, we show that ZnT3 associates with larger dendritic spines at synapses that also contain Shank3. Together, these results suggest that presynaptic vesicular

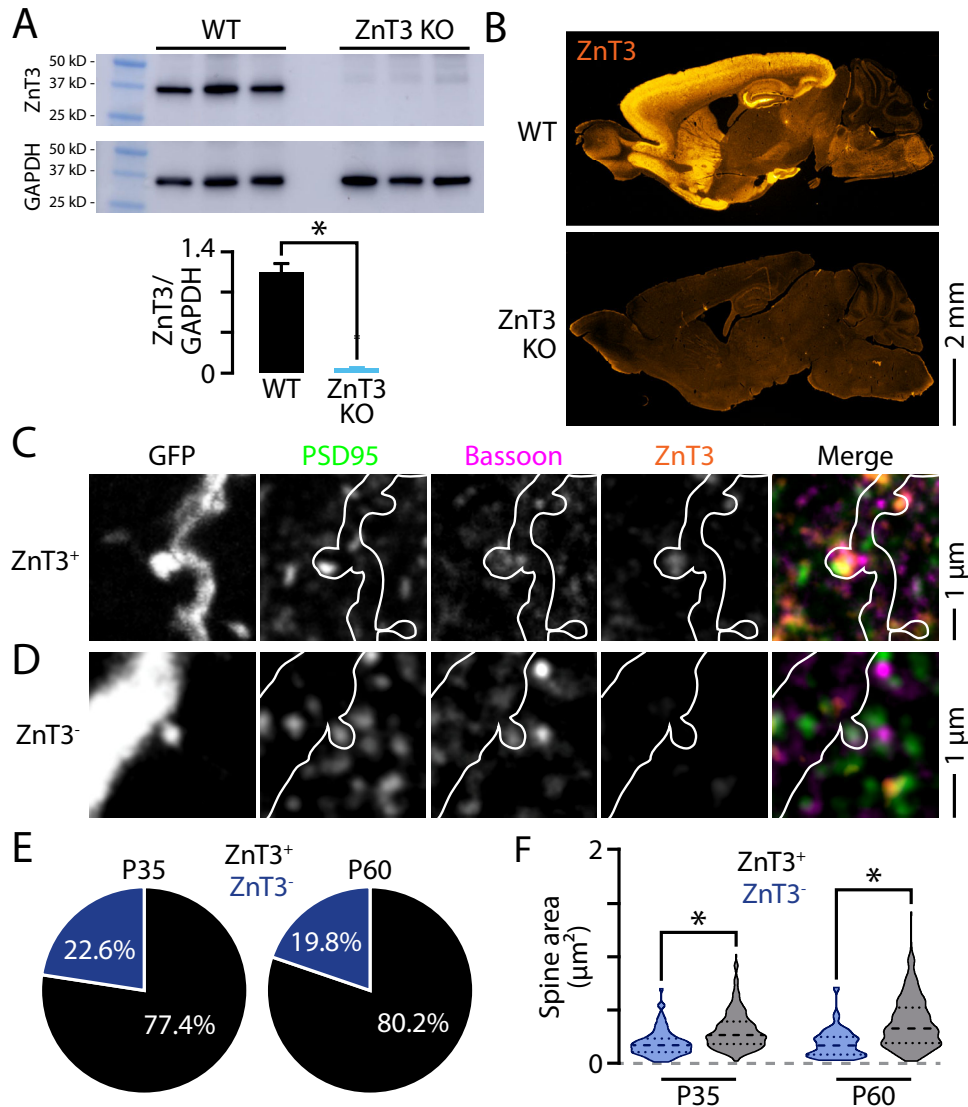


Figure 4. ZnT3 correlates with larger spines in WT mice. **A**, Top, Western blot bands for ZnT3 (top) and GAPDH (bottom) from WT and ZnT3 KO cortices. Bottom, Western blot quantification of the ZnT3 band intensity divided by the GAPDH band intensity ($p = 0.0130$; $n = 3$ mice; unpaired t test). **B**, Example images of a WT (top) and ZnT3 KO (bottom) mouse brain labeled for ZnT3. **C**, An example image of a synapse in Layer 2/3 of a WT mouse that expresses ZnT3. The white outline indicates the dendrite and dendritic spine. The merged image shows PSD-95 (green), bassoon (magenta), and ZnT3 (orange) stains. **D**, An example image of a synapse that does not express ZnT3. The same color scheme as in **C**. **E**, Pie charts showing the percentage of spines in Layer 2/3 of WT mice that either expressed (black) or did not express (blue) ZnT3 at both P35 (left) and P60 (right) (P35: $p = 1.47 \times 10^{-8}$; ZnT3⁺, $n = 333$ spines; ZnT3⁻, $n = 88$ spines; P60: $p < 1.00 \times 10^{-15}$; ZnT3⁺, $n = 311$ spines; ZnT3⁻, $n = 86$ spines; Kruskal–Wallis test with Dunn’s multiple comparisons).

zinc assists in the regulation of dendritic spine morphology and function through interactions with Shank3.

Zinc is highly enriched within synaptic vesicles in many brain regions by the vesicular zinc transporter protein ZnT3 (Palmiter et al., 1996; Cole et al., 1999; McAllister and Dyck, 2017a,b). Zinc is tightly regulated in the body through two families of proteins: zinc transporters that move zinc out of the cytoplasm and Zrt-/Irt-like proteins (ZIPs) that move zinc into the cytoplasm (Hershinkel et al., 2010; Kambe et al., 2015). Zinc ions can move into neurons through postsynaptic ZIPs (De Benedictis et al., 2021) or Ca²⁺-permeable channels such as voltage-gated calcium channels, calcium-permeable AMPARs, and NMDARs (Frederickson et al., 1989; Weiss et al., 1993; Koh and Choi, 1994; Yin and Weiss, 1995; Koh et al., 1996; Sensi et al., 1999). A defining aspect of Shank3 is its ability to self-associate with other Shank3 proteins through the SAM domain

(Naisbitt et al., 1999) and form tight sheets (Baron et al., 2006). Zn²⁺ stabilizes salt bridges between two SAM domains, causing highly mobile Shank3 pools to become more structured (Baron et al., 2006; Gundelfinger et al., 2006). Lack of the SAM domain in Shank3 is linked to a decrease in both the spine head size and mEPSC amplitudes (Durand et al., 2012). This decrease in mEPSC amplitude is consistent with decreases in mEPSC amplitude found in both Shank3 KO (Peça et al., 2011) and ZnT3 KO mice (Lavoie et al., 2011)—both of which display similar autism spectrum disorder-like phenotypes (Martel et al., 2011; Peça et al., 2011; Yoo et al., 2016; Thackray et al., 2017; Upmanyu et al., 2022). Our current findings suggest that presynaptic ZnT3-dependent zinc may contribute to these mechanisms and that changes in synaptic zinc availability and/or release may alter the ability of Shank3 proteins to self-associate and stabilize the postsynaptic density. Future studies directly linking presynaptic

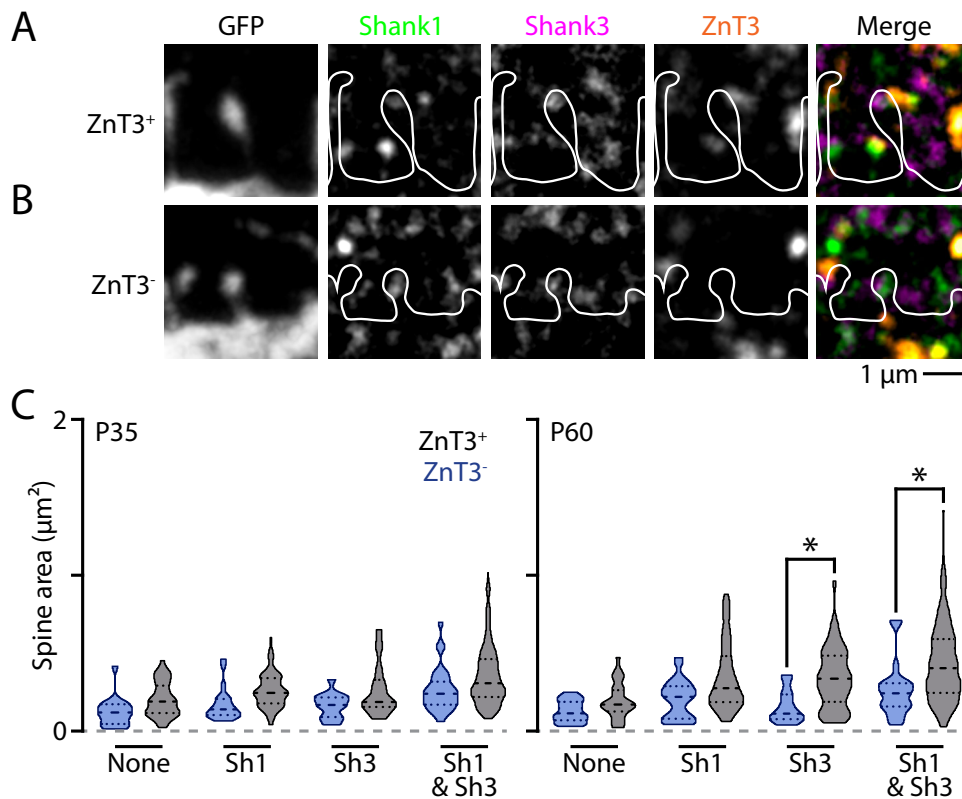


Figure 5. Spines with Shank3 are larger at synapses with ZnT3 at P60. **A**, An example image of a synapse in Layer 2/3 of a WT mouse that expresses ZnT3. The white outline indicates the dendrite and dendritic spine. The merged image shows Shank1 (green), Shank3 (magenta), and ZnT3 (orange) stains. **B**, An example image of a synapse that does not express ZnT3. The same color scheme as in **A**. **C**, The spine area for synapses in Layer 2/3 of a WT mouse that either expresses (black) or does not express (blue) ZnT3 at P35 (left) and P60 (right) for each condition (P35 none: $p > 0.999$; ZnT3⁺, $n = 333$ spines; ZnT3⁻, $n = 88$ spines; P35 Shank1: $p = 0.294$; ZnT3⁺, $n = 333$ spines; ZnT3⁻, $n = 88$ spines; P35 Shank3: $p > 0.999$; ZnT3⁺, $n = 333$ spines; ZnT3⁻, $n = 88$ spines; P35 Shank1/Shank3: $p > 0.999$; ZnT3⁺, $n = 333$ spines; ZnT3⁻, $n = 88$ spines; P60 none: $p > 0.999$; ZnT3⁺, $n = 333$ spines; ZnT3⁻, $n = 88$ spines; P60 Shank1: $p = 0.428$; ZnT3⁺, $n = 333$ spines; ZnT3⁻, $n = 88$ spines; P60 Shank3: $p = 0.0287$; ZnT3⁺, $n = 333$ spines, ZnT3⁻, $n = 88$ spines; P60 Shank1/Shank3: $p = 0.0000147$; ZnT3⁺, $n = 333$ spines; ZnT3⁻, $n = 88$ spines; Kruskal–Wallis with Dunn’s multiple-comparison test).

vesicular zinc to postsynaptic Shank3 self-association will be necessary to address this issue. One limitation of this study is the use of a germline KO of ZnT3 because ZnT3 KO mice display alterations in multiple aspects of brain development and sensory processing (Valente and Auladell, 2002; Yoo et al., 2016; Patrick Wu and Dyck, 2018; Kumar et al., 2019). Therefore, it is possible that factors related to developmental differences or sensory processing changes resulting from the genetic deletion of ZnT3 also contribute to synaptic changes in adult animals. Future experiments examining these possibilities will be required to address this important issue.

AMPA receptors are developmentally regulated glutamate-gated ion channels in the postsynaptic membrane that mediate fast excitatory transmission (Watkins and Evans, 1981; Honoré et al., 1982; Monaghan et al., 1989; Hollmann and Heinemann, 1994). The functional characteristics of AMPARs are determined by the specific combination of four subunits (GluA1–4) that form hetero-oligomers (Hollmann et al., 1991; Verdoorn et al., 1991; Traynelis et al., 2010). Shank3 assists in the trafficking of GluA2-containing AMPARs (Sheng and Kim, 2000; Bariselli et al., 2016; Ha et al., 2018) by binding to glutamate receptor-interacting protein—a scaffolding protein that binds to the C-terminus of GluA2 (Dong et al., 1997, 1999; Osten et al., 1998)—through Shank3’s Src homology 3 domain (Sheng and Kim, 2000). During development, synapses undergo a switch from inwardly rectifying (GluA2-lacking) AMPAR currents to

more nonrectifying (GluA2-containing) AMPAR currents (Bariselli et al., 2016; Ha et al., 2018). This shift is associated with an increase in Shank3 expression (Grabrucker et al., 2011a; Ha et al., 2018), suggesting that Shank3 contributes to this process. Because GluA2-lacking AMPARs also allow zinc influx (Sensi et al., 1999; Jia et al., 2002), our findings suggest that ZnT3-dependent zinc may contribute to the internalization of GluA2-lacking AMPARs by stabilizing Shank3 and enhancing the expression of GluA2-containing AMPARs at synapses. Future studies examining AMPAR rectification and subunit composition at ZnT3-containing versus ZnT3-lacking synapses during development will be required to answer these questions.

Long-term potentiation (LTP) is characterized by an increase in the spine head size (Fifková and Van Harreveld, 1977; Desmond and Levy, 1983; Matsuzaki et al., 2004), as well as an increase in AMPAR responses (Bliss and Lomo, 1973; Kauer et al., 1988; Bliss and Collingridge, 1993) and expression at the membrane (Isaac et al., 1995; Lissin et al., 1998; Shi et al., 1999; Y. Hayashi et al., 2000; Liao et al., 2001; Plant et al., 2006). Induction of NMDAR-dependent LTP leads to the rapid incorporation of inwardly rectifying GluA2-lacking AMPARs (Lissin et al., 1998; Shi et al., 1999; Y. Hayashi et al., 2000; Plant et al., 2006; Morita et al., 2014). Ca²⁺-permeable receptors allow a large amount of Ca²⁺ to flow into the cell and stimulate signaling pathways containing Ca²⁺-calmodulin-dependent protein kinase, phosphoinositide 3-kinase, mitogen-activated protein kinase,

protein kinase A, or mammalian target of rapamycin (Kelly et al., 2007). These signaling pathways increase translation of protein kinase M zeta, which upregulates interactions between NSF and GluA2 to increase AMPAR trafficking to the membrane (Kelly et al., 2007). As a synapse enters late-phase LTP, GluA2-containing AMPARs enter the membrane and replace GluA2-lacking AMPARs (Shi et al., 2001; Gardner et al., 2005; Plant et al., 2006; Morita et al., 2014). Shank3 KO mice have reduced excitatory postsynaptic potentials (EPSPs) during LTP induction and during late-phase LTP (M. Yang et al., 2012). Furthermore, Shank3 heterozygous mice have transiently increased EPSPs during the induction of LTP but are unable to maintain late-phase LTP because EPSP amplitude and spine volume return to the baseline (Bozdagi et al., 2010). These results indicate that Shank3 is necessary for maintaining late-phase LTP. Because Shank3 and free zinc assist in regulation of postsynaptic spine morphology (Grabrucker et al., 2011a, 2014; Arons et al., 2012, 2016; Hagemeyer et al., 2018; Vyas et al., 2020), our results suggest that presynaptic vesicular zinc supports late-phase LTP and its associated increase in the spine size. Together, these results suggest a mechanism for the development of larger spines at synapses that contain both ZnT3 and Shank3. Because zinc modulates LTP (Xie and Smart, 1994; Lu et al., 2000; Vogt et al., 2000; Li et al., 2001; Izumi et al., 2006; Kodirov et al., 2006; Pan et al., 2011; Sullivan et al., 2018; Morabito et al., 2022), our current findings suggest that synaptic zinc may also affect the morphological characteristics of spines during LTP in addition to the functional increase in synaptic receptor activity during LTP. Future work exploring the role of synaptic zinc, Shank3, and AMPAR subunits during late-phase LTP will be necessary to address these possibilities. Interactions between Shank3 and synaptic zinc are important components within a larger framework of molecules that supports dendritic spine morphology and function. Although our findings suggest an endogenous mechanism whereby vesicular zinc supports Shank3 and AMPAR function, there are numerous zinc-sensitive proteins (Hwang et al., 2005; Huang et al., 2008; Ha et al., 2018; Krall et al., 2022) and endogenous pools of zinc at and around synapses (Vogt et al., 2000; Vergnano et al., 2014; Anderson et al., 2015; Vogler et al., 2020; De Benedictis et al., 2021; Krall et al., 2022) that also influence synaptic function. Therefore, our findings offer an additional mechanistic link between presynaptic vesicular machinery and postsynaptic structural proteins within the larger network of cellular mechanisms that support normal synaptic structure and function in the brain.

References

- Actor-Engel HS, et al. (2021) Precision mapping of amyloid- β binding reveals perisynaptic localization and spatially restricted plasticity deficits. *eNeuro* 8:e2705–e2714.
- Adlard PA, Parncutt JM, Finkelstein DI, Bush AI (2010) Cognitive loss in zinc transporter-3 knock-out mice: a phenocopy for the synaptic and memory deficits of Alzheimer's disease? *J Neurosci* 30:1631–1636.
- Anderson CT, Radford RJ, Zastrow ML, Zhang DY, Apfel U-P, Lippard SJ, Tzounopoulos T (2015) Modulation of extrasynaptic NMDA receptors by synaptic and tonic zinc. *Proc Natl Acad Sci U S A* 112.
- Arellano JI (2007) Ultrastructure of dendritic spines: correlation between synaptic and spine morphologies. *Front Neurosci* 1:131–143.
- Arons MH, Lee K, Thynne CJ, Kim SA, Schob C, Kinder S, Montgomery JM, Garner CC (2016) Shank3 is part of a zinc-sensitive signaling system that regulates excitatory synaptic strength. *J Neurosci* 36:9124–9134.
- Arons MH, Thynne CJ, Grabrucker AM, Li D, Schoen M, Cheyne JE, Boeckers TM, Montgomery JM, Garner CC (2012) Autism-associated mutations in ProSAP2/Shank3 impair synaptic transmission and neurexin–neuroligin-mediated transsynaptic signaling. *J Neurosci* 32:14966–14978.
- Bariselli S, et al. (2016) SHANK3 controls maturation of social reward circuits in the VTA. *Nat Neurosci* 19:926–934.
- Baron MK, Boeckers TM, Vaida B, Faham S, Gingery M, Sawaya MR, Salyer D, Gundelfinger ED, Bowie JU (2006) An architectural framework that may lie at the core of the postsynaptic density. *Science* 311:531–535.
- Bats C, Groc L, Choquet D (2007) The interaction between stargazin and PSD-95 regulates AMPA receptor surface trafficking. *Neuron* 53:719–734.
- Bender PTR, McCollum M, Boyd-Pratt H, Mendelson BZ, Anderson CT (2023) Synaptic zinc potentiates AMPA receptor function in mouse auditory cortex. *Cell Rep* 42:112932.
- Bliss TVP, Collingridge GL (1993) A synaptic model of memory: long-term potentiation in the hippocampus. *Nature* 361:31–39.
- Bliss TVP, Lømo T (1973) Long-lasting potentiation of synaptic transmission in the dentate area of the anaesthetized rabbit following stimulation of the perforant path. *J Physiol* 232:331–356.
- Boccutto L, et al. (2013) Prevalence of SHANK3 variants in patients with different subtypes of autism spectrum disorders. *Eur J Hum Genet* 21:310–316.
- Borczyk M, Śliwińska MA, Caly A, Bernas T, Radwanska K (2019) Neuronal plasticity affects correlation between the size of dendritic spine and its postsynaptic density. *Sci Rep* 9:1693.
- Bozdagi O, et al. (2010) Haploinsufficiency of the autism-associated Shank3 gene leads to deficits in synaptic function, social interaction, and social communication. *Mol Autism* 1:15.
- Brown CE, Dyck RH (2004) Distribution of zincergic neurons in the mouse forebrain. *J Comp Neurol* 479:156–167.
- Cane M, Maco B, Knott G, Holtmaat A (2014) The relationship between PSD-95 clustering and spine stability in vivo. *J Neurosci* 34:2075–2086.
- Chang M, Kawai HD (2018) A characterization of laminar architecture in mouse primary auditory cortex. *Brain Struct Funct* 223:4187–4209.
- Chen T-W, et al. (2013) Ultrasensitive fluorescent proteins for imaging neuronal activity. *Nature* 499:295–300.
- Chen X, Levy JM, Hou A, Winters C, Azzam R, Sousa AA, Leapman RD, Nicoll RA, Reese TS (2015) PSD-95 family MAGUKs are essential for anchoring AMPA and NMDA receptor complexes at the postsynaptic density. *Proc Natl Acad Sci U S A* 112:e6983–e6992.
- Cody PA, Tzounopoulos T (2022) Neuromodulatory mechanisms underlying contrast gain control in mouse auditory cortex. *J Neurosci* 42:5564–5579.
- Cole TB, Wenzel HJ, Kafer KE, Schwartzkroin PA, Palmiter RD (1999) Elimination of zinc from synaptic vesicles in the intact mouse brain by disruption of the ZnT3 gene. *Proc Natl Acad Sci U S A* 96:1716–1721.
- Collins SM, Galvez R (2018) Neocortical SHANK1 regulation of forebrain dependent associative learning. *Neurobiol Learn Mem* 155:173–179.
- De Benedictis CA, Haffke C, Hagemeyer S, Sauer AK, Grabrucker AM (2021) Expression analysis of zinc transporters in nervous tissue cells reveals neuronal and synaptic localization of ZIP4. *Int J Mol Sci* 22:4511.
- De Rossi P, et al. (2020) Neuronal BIN1 regulates presynaptic neurotransmitter release and memory consolidation. *Cell Rep* 30:3520–3535.e7.
- Desmond NL, Levy WB (1983) Synaptic correlates of associative potentiation/depression: an ultrastructural study in the hippocampus. *Brain Res* 265:21–30.
- Dong H, O'Brien RJ, Fung ET, Lanahan AA, Worley PF, Huganir RL (1997) GRIP: a synaptic PDZ domain-containing protein that interacts with AMPA receptors. *Nature* 386:279–284.
- Dong H, Zhang P, Song I, Petralia RS, Liao D, Huganir RL (1999) Characterization of the glutamate receptor-interacting proteins GRIP1 and GRIP2. *J Neurosci* 19:6930–6941.
- Du Y, Weed SA, Xiong W-C, Marshall TD, Parsons JT (1998) Identification of a novel cortactin SH3 domain-binding protein and its localization to growth cones of cultured neurons. *Mol Cell Biol* 18:5838–5851.
- Dumitriu D, Hao J, Hara Y, Kaufmann J, Janssen WGM, Lou W, Rapp PR, Morrison JH (2010) Selective changes in thin spine density and morphology in monkey prefrontal cortex correlate with aging-related cognitive impairment. *J Neurosci* 30:7507–7515.
- Durand CM, Perroy J, Loll F, Perrais D, Fagni L, Bourgeron T, Montcouquiol M, Sans N (2012) SHANK3 mutations identified in autism lead to modification of dendritic spine morphology via an actin-dependent mechanism. *Mol Psychiatry* 17:71–84.
- Engert F, Bonhoeffer T (1999) Dendritic spine changes associated with hippocampal long-term synaptic plasticity. *Nature* 399:66–70.

- Feng B, Freitas AE, Gorodetski L, Wang J, Tian R, Lee YR, Grewal AS, Zou Y (2021) Planar cell polarity signaling components are a direct target of β -amyloid-associated degeneration of glutamatergic synapses. *Sci Adv* 7:eabh2307.
- Fifiková E, Van Harreveld A (1977) Long-lasting morphological changes in dendritic spines of dentate granular cells following stimulation of the entorhinal area. *J Neurocytol* 6:211–230.
- Frederickson CJ, Hernandez MD, McGinty JF (1989) Translocation of zinc may contribute to seizure-induced death of neurons. *Brain Res* 480:317–321.
- Gardner SM, Takamiya K, Xia J, Suh J-G, Johnson R, Yu S, Huganir RL (2005) Calcium-permeable AMPA receptor plasticity is mediated by subunit-specific interactions with PICK1 and NSF. *Neuron* 45:903–915.
- Ghani MU, Mesadi F, Kanik SD, Argunşah AÖ, Hobbiss AF, Israely I, Ünay D, Taşdizen T, Çetin M (2017) Dendritic spine classification using shape and appearance features based on two-photon microscopy. *J Neurosci Methods* 279:13–21.
- Grabrucker AM, et al. (2011a) Concerted action of zinc and ProSAP/Shank in synaptogenesis and synapse maturation: ProSAPs in synaptogenesis and synapse maturation. *EMBO J* 30:569–581.
- Grabrucker S, et al. (2014) Zinc deficiency dysregulates the synaptic ProSAP/Shank scaffold and might contribute to autism spectrum disorders. *Brain* 137:137–152.
- Grabrucker AM, Schmeisser MJ, Schoen M, Boeckers TM (2011b) Postsynaptic ProSAP/Shank scaffolds in the cross-hair of synaptopathies. *Trends Cell Biol* 21:594–603.
- Grutzendler J, Kasthuri N, Gan W-B (2002) Long-term dendritic spine stability in the adult cortex. *Nature* 420:812–816.
- Gundelfinger ED, Boeckers TM, Baron MK, Bowie JU (2006) A role for zinc in postsynaptic density assembly and plasticity? *Trends Biochem Sci* 31:366–373.
- Ha HTT, Leal-Ortiz S, Lalwani K, Kiyonaka S, Hamachi I, Mysore SP, Montgomery JM, Garner CC, Huguenard JR, Kim SA (2018) Shank and zinc mediate an AMPA receptor subunit switch in developing neurons. *Front Mol Neurosci* 11:405.
- Hagmeyer S, Sauer AK, Grabrucker AM (2018) Prospects of zinc supplementation in autism spectrum disorders and shankopathies such as Phelan McDermid syndrome. *Front Synaptic Neurosci* 10:11.
- Harris K, Jensen F, Tsao B (1992) Three-dimensional structure of dendritic spines and synapses in rat hippocampus (CA1) at postnatal day 15 and adult ages: implications for the maturation of synaptic physiology and long-term potentiation. *J Neurosci* 12:2685–2705. [published erratum appears in *J Neurosci* 1992 Aug;12(8):following table of contents].
- Harris K, Stevens J (1989) Dendritic spines of CA1 pyramidal cells in the rat hippocampus: serial electron microscopy with reference to their biophysical characteristics. *J Neurosci* 9:2982–2997.
- Harvey CD, Svoboda K (2007) Locally dynamic synaptic learning rules in pyramidal neuron dendrites. *Nature* 450:1195–1200.
- Hayashi Y, Shi S-H, Esteban JA, Piccini A, Poncer J-C, Malinow R (2000) Driving AMPA receptors into synapses by LTP and CaMKII: requirement for GluR1 and PDZ domain interaction. *Science* 287:2262–2267.
- Hayashi MK, Tang C, Verpelli C, Narayanan R, Stearns MH, Xu R-M, Li H, Sala C, Hayashi Y (2009) The postsynaptic density proteins homer and shank form a polymeric network structure. *Cell* 137:159–171.
- He CX, Arroyo ED, Cantu DA, Goel A, Portera-Cailliau C (2018) A versatile method for viral transfection of calcium indicators in the neonatal mouse brain. *Front Neural Circuits* 12:56.
- Hershfkinkel M, Aizenman E, Andrews G, Sekler I (2010) Zinc bells rang in Jerusalem! A report on the meeting of the international society for zinc biology, Jerusalem, Israel, 1 to 5 December 2009. *Sci Signal* 3:1–7.
- Hollmann M, Hartley M, Heinemann S (1991) Ca^{2+} permeability of KA-AMPA-gated glutamate receptor channels depends on subunit composition. *Science* 252:851–853.
- Hollmann M, Heinemann S (1994) Cloned glutamate receptors. *Annu Rev Neurosci* 17:31–108.
- Honoré T, Lauridsen J, Krogsgaard-Larsen P (1982) The binding of [3H] AMPA, a structural analogue of glutamic acid, to rat brain membranes. *J Neurochem* 38:173–178.
- Hooks BM, Hires SA, Zhang Y-X, Huber D, Petreanu L, Svoboda K, Shepherd GMG (2011) Laminar analysis of excitatory local circuits in vibrissal motor and sensory cortical areas (Petersons CCCH, ed). *PLoS Biol* 9:e1000572.
- Hruska M, Cain RE, Dalva MB (2022) Nanoscale rules governing the organization of glutamate receptors in spine synapses are subunit specific. *Nat Commun* 13:920.
- Hruska M, Henderson N, Le Marchand SJ, Jafri H, Dalva MB (2018) Synaptic nanomodules underlie the organization and plasticity of spine synapses. *Nat Neurosci* 21:671–682.
- Huang YZ, Pan E, Xiong Z-Q, McNamara JO (2008) Zinc-mediated transactivation of TrkB potentiates the hippocampal mossy fiber-CA3 pyramidal synapse. *Neuron* 57:546–558.
- Hwang JJ, Park M-H, Choi S-Y, Koh J-Y (2005) Activation of the trk signaling pathway by extracellular zinc. *J Biol Chem* 280:11995–12001.
- Isaac JTR, Nicoll RA, Malenka RC (1995) Evidence for silent synapses: implications for the expression of LTP. *Neuron* 15:427–434.
- Ishii K, Nagaoka A, Kishida Y, Okazaki H, Yagishita S, Ucar H, Takahashi N, Saito N, Kasai H (2018) In vivo volume dynamics of dendritic spines in the neocortex of wild-type and *Fmr1* KO mice. *eNeuro* 5:0282–18.2018.
- Izumi Y, Auberson YP, Zorumski CF (2006) Zinc modulates bidirectional hippocampal plasticity by effects on NMDA receptors. *J Neurosci* 26:7181–7188.
- Jia Y, Jeng J, Sensi SL, Weiss JH (2002) Zn^{2+} currents are mediated by calcium-permeable AMPA/Kainate channels in cultured murine hippocampal neurons. *J Physiol* 543:35–48.
- Joshi A, Middleton JW, Anderson CT, Borges K, Suter BA, Shepherd GMG, Tzounopoulos T (2015) Cell-specific activity-dependent fractionation of layer 2/3->5B excitatory signaling in mouse auditory cortex. *J Neurosci* 35:3112–3123.
- Kalappa BI, Anderson CT, Goldberg JM, Lippard SJ, Tzounopoulos T (2015) AMPA receptor inhibition by synaptically released zinc. *Proc Natl Acad Sci U S A* 112:15749–15754.
- Kalappa BI, Tzounopoulos T (2017) Context-dependent modulation of excitatory synaptic strength by synaptically released zinc. *eNeuro* 4:ENEURO.0011-17.2017.
- Kambe T, Tsuji T, Hashimoto A, Isumura N (2015) The physiological, biochemical, and molecular roles of zinc transporters in zinc homeostasis and metabolism. *Physiol Rev* 95:749–784.
- Kang M, Lee D, Song J, Park S, Park D, Lee S, Suh YH (2021) Neddylation is required for presynaptic clustering of mGlu7 and maturation of presynaptic terminals. *Exp Mol Med* 53:457–467.
- Kauer JA, Malenka RC, Nicoll RA (1988) A persistent postsynaptic modification mediates long-term potentiation in the hippocampus. *Neuron* 1:911–917.
- Kelly MT, Cray JF, Sacktor TC (2007) Regulation of protein kinase M ζ synthesis by multiple kinases in long-term potentiation. *J Neurosci* 27:3439–3444.
- Kilisch M, Gere-Becker M, Wüstefeld L, Bonnas C, Crauel A, Mechmershausen M, Martens H, Götzke H, Opazo F, Frey S (2023) Simple and highly efficient detection of PSD95 using a nanobody and its recombinant heavy-chain antibody derivatives. *Int J Mol Sci* 24:7294.
- Kim E, Sheng M (2004) PDZ domain proteins of synapses. *Nat Rev Neurosci* 5:771–781.
- Kodirov SA, Takizawa S, Joseph J, Kandel ER, Shumyatsky GP, Bolshakov VY (2006) Synaptically released zinc gates long-term potentiation in fear conditioning pathways. *Proc Natl Acad Sci U S A* 103:15218–15223.
- Koh J-Y, Choi DW (1994) Zinc toxicity on cultured cortical neurons: involvement of N-methyl-D-aspartate receptors. *Neuroscience* 60:1049–1057.
- Koh J-Y, Suh SW, Gwag BJ, He YY, Hsu CY, Choi DW (1996) The role of zinc in selective neuronal death after transient global cerebral ischemia. *Science* 272:1013–1016.
- Kornau H-C, Schenker LT, Kennedy MB, Seeburg PH (1995) Domain interaction between NMDA receptor subunits and the postsynaptic density protein PSD-95. *Science* 269:1737–1740.
- Krall R, Gale JR, Ross MM, Tzounopoulos T, Aizenman E (2022) Intracellular zinc signaling influences NMDA receptor function by enhancing the interaction of ZnT1 with GluN2A. *Neurosci Lett* 790:136896.
- Kumar M, Xiong S, Tzounopoulos T, Anderson CT (2019) Fine control of sound frequency tuning and frequency discrimination acuity by synaptic zinc signaling in mouse auditory cortex. *J Neurosci* 39:854–865.
- Lavoie N, Jeyaraju DV, Peralta MR, Seress L, Pellegrini L, Toth K (2011) Vesicular zinc regulates the Ca^{2+} sensitivity of a subpopulation of presynaptic vesicles at hippocampal mossy fiber terminals. *J Neurosci* 31:18251–18265.
- Li Y, Hough CJ, Frederickson CJ, Sarvey JM (2001) Induction of mossy fiber-CA3 long-term potentiation requires translocation of synaptically released Zn^{2+} . *J Neurosci* 21:8015–8025.
- Liao D, Scannevin RH, Huganir R (2001) Activation of silent synapses by rapid activity-dependent synaptic recruitment of AMPA receptors. *J Neurosci* 21:6008–6017.

- Lissin DV, Gomperts SN, Carroll RC, Christine CW, Kalman D, Kitamura M, Hardy S, Nicoll RA, Malenka RC, Von Zastrow M (1998) Activity differentially regulates the surface expression of synaptic AMPA and NMDA glutamate receptors. *Proc Natl Acad Sci U S A* 95:7097–7102.
- Liu S-QJ, Cull-Candy SG (2000) Synaptic activity at calcium-permeable AMPA receptors induces a switch in receptor subtype. *Nature* 405:454–458.
- Liu C, Kershberg L, Wang J, Schneeberger S, Kaeser PS (2018) Dopamine secretion is mediated by sparse active zone-like release sites. *Cell* 172:706–718.e15.
- Loureiro LO, et al. (2021) A recurrent SHANK3 frameshift variant in autism spectrum disorder. *NPJ Genom Med* 6:91.
- Lu Y-M, Taverna FA, Tu R, Ackerley CA, Wang Y-T, Roder J (2000) Endogenous Zn²⁺ is required for the induction of long-term potentiation at rat hippocampal mossy fiber-CA3 synapses. *Synapse* 38:187–197.
- Magupalli VG, Schwarz K, Alpadi K, Natarajan S, Seigel GM, Schmitz F (2008) Multiple RIBEYE-RIBEYE interactions create a dynamic scaffold for the formation of synaptic ribbons. *J Neurosci* 28:7954–7967.
- Maletic-Savatic M, Malinow R, Svoboda K (1999) Rapid dendritic morphogenesis in CA1 hippocampal dendrites induced by synaptic activity. *Science* 283:1923–1927.
- Man W, et al. (2020) SHANK3 co-ordinately regulates autophagy and apoptosis in myocardial infarction. *Front Physiol* 11:1082.
- Martel G, Hevi C, Friebely O, Baybutt T, Shumyatsky GP (2010) Zinc transporter 3 is involved in learned fear and extinction, but not in innate fear. *Learn Mem* 17:582–590.
- Martel G, Hevi C, Kane-Goldsmith N, Shumyatsky GP (2011) Zinc transporter ZnT3 is involved in memory dependent on the hippocampus and perirhinal cortex. *Behav Brain Res* 223:233–238.
- Matsuzaki M, Ellis-Davies GCR, Nemoto T, Miyashita Y, Iino M, Kasai H (2001) Dendritic spine geometry is critical for AMPA receptor expression in hippocampal CA1 pyramidal neurons. *Nat Neurosci* 4:1086–1092.
- Matsuzaki M, Honkura N, Ellis-Davies GCR, Kasai H (2004) Structural basis of long-term potentiation in single dendritic spines. *Nature* 429:761–766.
- McAllister BB, Dyck RH (2017a) Zinc transporter 3 (ZnT3) and vesicular zinc in central nervous system function. *Neurosci Biobehav Rev* 80:329–350.
- McAllister BB, Dyck RH (2017b) A new role for zinc in the brain. *Elife* 6:e31816.
- Moessner R, et al. (2007) Contribution of SHANK3 mutations to autism spectrum disorder. *Am J Hum Genet* 81:1289–1297.
- Monaghan DT, Bridges RJ, Cotman CW (1989) The excitatory amino acid receptors: their classes, pharmacology, and distinct properties in the function of the central nervous system. *Annu Rev Pharmacol Toxicol* 29:365–402.
- Morabito A, Zerlaut Y, Serraz B, Sala R, Paoletti P, Rebola N (2022) Activity-dependent modulation of NMDA receptors by endogenous zinc shapes dendritic function in cortical neurons. *Cell Rep* 38:110415.
- Morita D, Rah JC, Isaac JTR (2014) Incorporation of inwardly rectifying AMPA receptors at silent synapses during hippocampal long-term potentiation. *Philos Trans R Soc B Biol Sci* 369:20130156.
- Naisbitt S, Kim E, Tu JC, Xiao B, Sala C, Valtchanoff J, Weinberg RJ, Worley PF, Sheng M (1999) Shank, a novel family of postsynaptic density proteins that binds to the NMDA receptor/PSD-95/GKAP complex and cortactin. *Neuron* 23:569–582.
- Oray S, Majewska A, Sur M (2006) Effects of synaptic activity on dendritic spine motility of developing cortical layer V pyramidal neurons. *Cereb Cortex* 16:730–741.
- Orner DA, Chen C-C, Orner DE, Brumberg JC (2014) Alterations of dendritic protrusions over the first postnatal year of a mouse: an analysis in layer VI of the barrel cortex. *Brain Struct Funct* 219:1709–1720.
- Osten P, et al. (1998) The AMPA receptor GluR2 C terminus can mediate a reversible, ATP-dependent interaction with NSF and α - and β -SNAPs. *Neuron* 21:99–110.
- Palmiter RD, Cole TB, Quaife CJ, Findley SD (1996) ZnT-3, a putative transporter of zinc into synaptic vesicles. *Proc Natl Acad Sci U S A* 93:14934–14939.
- Pan E, Zhang X, Huang Z, Krezel A, Zhao M, Tinberg CE, Lippard SJ, McNamara JO (2011) Vesicular zinc promotes presynaptic and inhibits postsynaptic long-term potentiation of mossy fiber-CA3 synapse. *Neuron* 71:1116–1126.
- Patrick Wu H-P, Dyck RH (2018) Signaling by synaptic zinc is required for whisker-mediated, fine texture discrimination. *Neuroscience* 369:242–247.
- Peça J, Feliciano C, Ting JT, Wang W, Wells MF, Venkatraman TN, Lascola CD, Fu Z, Feng G (2011) Shank3 mutant mice display autistic-like behaviours and striatal dysfunction. *Nature* 472:437–442.
- Petralia RS, Esteban JA, Wang Y-X, Partridge JG, Zhao H-M, Wenthold RJ, Malinow R (1999) Selective acquisition of AMPA receptors over postnatal development suggests a molecular basis for silent synapses. *Nat Neurosci* 2:31–36.
- Petreanu L, Huber D, Sobczyk A, Svoboda K (2007) Channelrhodopsin-2-assisted circuit mapping of long-range callosal projections. *Nat Neurosci* 10:663–668.
- Plant K, Pelkey KA, Bortolotto ZA, Morita D, Terashima A, McBain CJ, Collingridge GL, Isaac JTR (2006) Transient incorporation of native GluR2-lacking AMPA receptors during hippocampal long-term potentiation. *Nat Neurosci* 9:602–604.
- Sala C, Vicidomini C, Bigi I, Mossa A, Vercelli C (2015) Shank synaptic scaffold proteins: keys to understanding the pathogenesis of autism and other synaptic disorders. *J Neurochem* 135:849–858.
- Salazar G, Craige B, Love R, Kalman D, Faundez V (2005) Vglut1 and ZnT3 co-targeting mechanisms regulate vesicular zinc stores in PC12 cells. *J Cell Sci* 118:1911–1921.
- Schindelin J, et al. (2012) Fiji: an open-source platform for biological-image analysis. *Nat Methods* 9:676–682.
- Sensi SL, Yin HZ, Weiss JH (1999) Glutamate triggers preferential Zn²⁺ flux through Ca²⁺-permeable AMPA channels and consequent ROS production. *Neuroreport* 10:1723–1727.
- Sheng M, Kim E (2000) The shank family of scaffold proteins. *J Cell Sci* 113:1851–1856.
- Shi S-H, Hayashi Y, Esteban JA, Malinow R (2001) Subunit-specific rules governing AMPA receptor trafficking to synapses in hippocampal pyramidal neurons. *Cell* 105:331–343.
- Shi S-H, Hayashi Y, Petralia RS, Zaman SH, Wenthold RJ, Svoboda K, Malinow R (1999) Rapid spine delivery and redistribution of AMPA receptors after synaptic NMDA receptor activation. *Science* 284:1811–1816.
- Sullivan JA, Zhang X, Sullivan AP, Vose LR, Moghadam AA, Fried VA, Stanton PK (2018) Zinc enhances hippocampal long-term potentiation at CA1 synapses through NR2B containing NMDA receptors (Adams MM, ed). *PLoS One* 13:e0205907.
- Suter B, O'Connor T, Iyer V, Petreanu LT, Hooks BM, Kiritani T, Svoboda K, Shepherd GM (2010) Ephus: multipurpose data acquisition software for neuroscience experiments. *Front Neural Circuits* 4:1–12.
- Takao-Rikitsu E, Mochida S, Inoue E, Deguchi-Tawarada M, Inoue M, Ohtsuka T, Takai Y (2004) Physical and functional interaction of the active zone proteins, CAST, RIM1, and Bassoon, in neurotransmitter release. *J Cell Biol* 164:301–311.
- Takumi Y, Ramírez-León V, Laake P, Rinivik E, Ottersen OP (1999) Different modes of expression of AMPA and NMDA receptors in hippocampal synapses. *Nat Neurosci* 2:618–624.
- Thackray SE, McAllister BB, Dyck RH (2017) Behavioral characterization of female zinc transporter 3 (ZnT3) knockout mice. *Behav Brain Res* 321:36–49.
- Tom Dieck S, Altmann WD, Kessels MM, Qualmann B, Regus H, Brauner D, Fejtová A, Bracko O, Gundelfinger ED, Brandstätter JH (2005) Molecular dissection of the photoreceptor ribbon synapse. *J Cell Biol* 168:825–836.
- Traynelis SF, Wollmuth LP, McBain CJ, Menniti FS, Vance KM, Ogden KK, Hansen KB, Yuan H, Myers SJ, Dingledine R (2010) Glutamate receptor ion channels: structure, regulation, and function (Sibley D, ed). *Pharmacol Rev* 62:405–496.
- Uchino S, Waga C (2013) SHANK3 as an autism spectrum disorder-associated gene. *Brain Dev* 35:106–110.
- Upmanyu N, et al. (2022) Colocalization of different neurotransmitter transporters on synaptic vesicles is sparse except for VGLUT1 and ZnT3. *Neuron* 110:1483–1497.e7.
- Valente T, Auladell C (2002) Developmental expression of ZnT3 in mouse brain: correlation between the vesicular zinc transporter protein and chelatable vesicular zinc (CVZ) cells. Glial and neuronal CVZ cells interact. *Mol Cell Neurosci* 21:189–204.
- Verdoorn TA, Burnashev N, Monyer H, Seeburg PH, Sakmann B (1991) Structural determinants of ion flow through recombinant glutamate receptor channels. *Science* 252:1715–1718.
- Vergnano AM, Rebola N, Savtchenko LP, Pinheiro PS, Casado M, Kieffer BL, Rusakov DA, Mülle C, Paoletti P (2014) Zinc dynamics and action at excitatory synapses. *Neuron* 82:1101–1114.

- Vogler NW, Betti VM, Goldberg JM, Tzounopoulos T (2020) Mechanisms underlying long-term synaptic zinc plasticity at mouse dorsal cochlear nucleus glutamatergic synapses. *J Neurosci* 40:4981–4996.
- Vogt K, Mellor J, Tong G, Nicoll R (2000) The actions of synaptically released zinc at hippocampal mossy fiber synapses. *Neuron* 26:187–196.
- Vyas Y, Lee K, Jung Y, Montgomery JM (2020) Influence of maternal zinc supplementation on the development of autism-associated behavioural and synaptic deficits in offspring *Shank3*-knockout mice. *Mol Brain* 13:110.
- Wang Y-Z, Perez-Rosello T, Surmeier DJ, Savas JN (2023) Neuron-specific protein expression at striatal excitatory synapses. Available at: <http://biorxiv.org/lookup/doi/10.1101/2023.03.16.532957> [Accessed May 13, 2024].
- Watkins JC, Evans RH (1981) Excitatory amino acid transmitters. *Annu Rev Pharmacol Toxicol* 21:165–204.
- Weiss JH, Hartley DM, Koh J, Choi DW (1993) AMPA receptor activation potentiates zinc neurotoxicity. *Neuron* 10:43–49.
- Won S, Incontro S, Nicoll RA, Roche KW (2016) PSD-95 stabilizes NMDA receptors by inducing the degradation of STEP₆₁. *Proc Natl Acad Sci U S A* 113:e4736–e4744.
- Won S, Levy JM, Nicoll RA, Roche KW (2017) MAGUKs: multifaceted synaptic organizers. *Curr Opin Neurobiol* 43:94–101.
- Xie X, Smart TG (1994) Modulation of long-term potentiation in rat hippocampal pyramidal neurons by zinc. *Pflugers Arch* 427:481–486.
- Xue Q, Varady SRS, Waddell TQA, Roman MR, Carrington J, Roh-Johnson M (2023) Lack of Paxillin phosphorylation promotes single-cell migration in vivo. *J Cell Biol* 222:e202206078.
- Yang M, et al. (2012) Reduced excitatory neurotransmission and mild autism-relevant phenotypes in adolescent *Shank3* null mutant mice. *J Neurosci* 32:6525–6541.
- Yang Y, Wang X, Frerking M, Zhou Q (2008) Spine expansion and stabilization associated with long-term potentiation. *J Neurosci* 28:5740–5751.
- Yin HZ, Weiss JH (1995) Zn²⁺-permeable Ca²⁺-permeable AMPA/kainate channels and triggers selective neural injury. *Neuroreport* 6:2553–2556.
- Yoo MH, Kim T-Y, Yoon YH, Koh J-Y (2016) Autism phenotypes in ZnT3 null mice: involvement of zinc dyshomeostasis, MMP-9 activation and BDNF upregulation. *Sci Rep* 6:28548.
- Young ME, Ohm DT, Dumitriu D, Rapp PR, Morrison JH (2014) Differential effects of aging on dendritic spines in visual cortex and prefrontal cortex of the rhesus monkey. *Neuroscience* 274:33–43.
- Ziv NE, Smith SJ (1996) Evidence for a role of dendritic filopodia in synaptogenesis and spine formation. *Neuron* 17:91–102.